An explanation for the shape of Earth's gravity spectrum based on viscous mantle flow models

Bernhard Steinberger

Cooperative Institute for Research in Environmental Sciences (CIRES), University of Colorado, Boulder, Colorado, USA

Richard Holme

Department of Earth Sciences, University of Liverpool, Liverpool, UK

Received 13 May 2002; revised 27 June 2002; accepted 10 July 2002; published 7 November 2002.

[1] The Earth's gravity spectrum can be used as an observational constraint on geophysical modelling. Here we show how the spectrum up to degree $l = 31$ can be explained to a large part by viscous mantle flow in combination with a very simple model of random mantle density anomalies. Efforts to make the calculation more "realistic" by considering effects of thermal boundary layers, or using density anomalies based on tomography, or geodynamic modelling, tend to worsen the fit. Results are rather sensitive to assumptions on density anomalies in the upper thermal boundary layer. We suggest that, in combination with other observations, the shape of the Earth's gravity spectrum can serve to better constrain radial viscosity structure, density anomalies and flow in the Earth's mantle. Appropriate treatment of the lithosphere and of lateral viscosity variations will be the main challenges in modelling this spectrum. *INDEX TERMS:* 1213 Geodesy and Gravity: Earth's interior—dynamics (8115, 8120); 8120 Tectonophysics: Dynamics of lithosphere and mantle—general; 8122 Tectonophysics: Dynamics, gravity and tectonics; 8121 Tectonophysics: Dynamics, convection currents and mantle plumes; 8162 Tectonophysics: Evolution of the Earth: Rheology—mantle. **Citation:** Steinberger, B., and R. Holme, An explanation for the shape of Earth's gravity spectrum based on viscous mantle flow models, *Geophys. Res. Lett.*, *29*(21), 2019, doi:10.1029/2002GL015476, 2002.

1. Introduction

[2] Although following the work of *Richards and Hager* [1984] and others, the Earth's geoid and gravity field have frequently been used to constrain mantle flow, the shape of the Earth's gravity spectrum has been only rarely used. Recently, *Hipkin* [2001] showed that, with an appropriate definition, the gravity spectrum shows several distinct features; hence it can be expected that, by comparing the geoid spectrum predicted from geodynamic models with the observed spectrum, additional insight can be gained: He defined the average dimensionless gravity power $\langle P_l \rangle$ of each spherical harmonic component of degree l

$$\langle P_l \rangle = (l+1)\left(C_l^{02} + \sum_{m=1}^{l}\left(C_l^{m2} + S_l^{m2}\right)\right) \qquad (1)$$

where $\{C_l^m, S_l^m\}$ are fully normalized spherical harmonic expansion coefficients of the gravity potential, made dimensionless by dividing by GM/r_E, where GM is the geocentric gravitational constant and r_E is the Earth radius. On a log-linear plot, this quantity shows breaks in slope at harmonic degrees $l \approx 12$ [*Kaula*, 1980], 4 and 30. *Hipkin* [2001] modelled this spectrum as the sum of four white noise sources at different depths within the Earth, one in the lithosphere (50 km depth) and three sub-lithosphere (315 km, 1280 km, >2750 km). Here we extend this work by showing that the shape of the spectrum can in fact be expected for a simple model of convection in a viscous mantle.

0094-8276/02/2002GL015476$05.00

2. Model Description

[3] We treat the Earth's mantle as a highly viscous fluid, an approximation which seems appropriate for the Earth's sublithospheric mantle, and has been very successful in explaining the Earth's geoid [e.g., *Hager and Richards*, 1989], but which is probably not adequate for the lithosphere. We also assume whole mantle flow, i.e. any density anomaly drives a flow component in the entire mantle. The approach of computing viscous flow and resulting gravity used here is essentially the same as developed by *Richards and Hager* [1984]. We assume viscous rheology for the lithosphere with a free upper boundary. We include effects of compressibility and phase boundaries, as in *Steinberger* [2000]. However, we assume that mantle viscosity depends on depth only.

[4] With our assumptions, C_l^m and S_l^m can be related to the density expansion coefficients $\delta\rho_{cl}^m(r)$ and $\delta\rho_{sl}^m(r)$ through geoid kernels $K_l(r)$:

$$C_l^m = \frac{3}{(2l+1)\bar{\rho}r_E}\int_{r_{CMB}}^{r_E} K_l(r)\delta\rho_{cl}^m(r)dr \qquad (2)$$

and likewise for S_l^m. $\bar{\rho}$ is the average density of the Earth, and r_{CMB} is the radius of the core-mantle boundary. The geoid kernels sum up the effect of the mantle density anomalies themselves, and of the deflection of boundaries, especially the Earth's surface and the core-mantle boundary, resulting from flow induced by these density anomalies.

[5] For most calculations, we use a radial mantle viscosity profile derived by *Steinberger and Calderwood* [2001], which is based on current knowledge of the mineral physics of mantle materials, explains large parts of the geoid, gives a realistic radial heat flow profile, and predicts slow motions of hotspots in accord with observed hotspot tracks (see *Steinberger and O'Connell* [1998], where a similar profile was proposed). In addition, we also use other viscosity profiles (Figure 1). Most of these were derived by fitting the geoid.

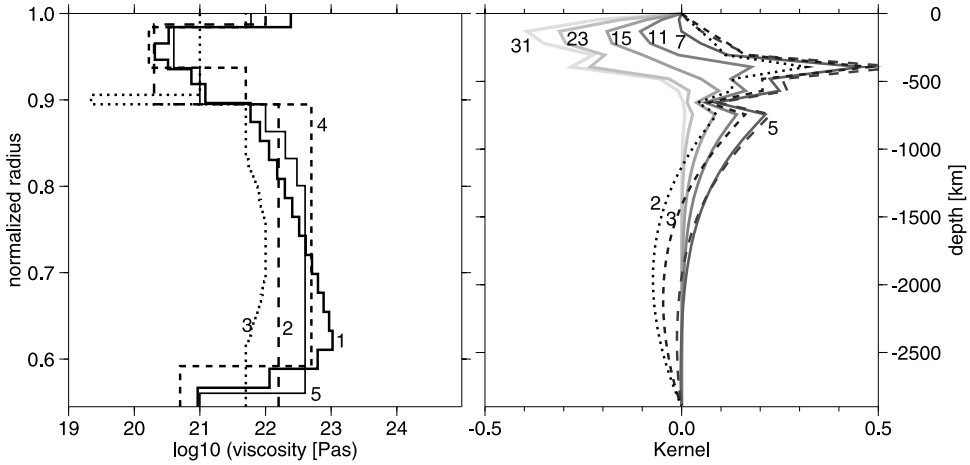

Figure 1. Left panel: Viscosity profiles used. (1): *Steinberger and Calderwood* [2001] (2): *Thoraval and Richards* [1997] (3): *Forte et al.* [1993] (4): *Hager and Richards* [1989] (5): *Steinberger* [2000] Right panel: Geoid kernels $K_l(r)$ as defined in equation (2) for viscosity profile (1). Degree l is indicated at each curve. The kinks of the kernels result from phase boundaries, which are treated as in *Steinberger* [2000].

[6] The following density structures are considered:

1. Random density structure: The mantle is divided into $N = 33$ layers of equal thickness. In each layer, coefficients $\delta\rho_{cl}^m$ and $\delta\rho_{sl}^m$ are assumed to be taken from a normal distribution with zero mean and standard deviation

$$\sigma(l) = \widehat{\Delta\rho} \cdot \rho_0(r_i)\sqrt{N/[l(l+1)(2l+1)]} \tag{3}$$

unless stated otherwise. $\rho_0(r_i)$ is the PREM [*Dziewonski and Anderson*, 1981] density at the radius r_i of layer i, and $\widehat{\Delta\rho}$ is a measure of relative density variations, assumed to be independent of radius. A spectral dependence $\propto 1/\sqrt{(l+1)(2l+1)}$ commonly approximates seismic tomography models [*Becker and Boschi*, 2001, Figure 2]. The additional factor $1/\sqrt{l}$ is introduced to account for radial correlation between layers. We expect the radial extent of an anomaly to be proportional to its lateral extent. Thus the effective layer thickness at degree l, and the consequent amplitude of its mass anomaly A_l, is proportional to $1/l$. The number of such layers within the mantle n_l is inversely proportional to their thickness, so $n_l \propto l$. The cumulative amplitude over n radial layers is expected to be $\sqrt{n}$ times that of a single layer. Thus the overall amplitude for anomalies at degree l is $\sqrt{n_l}A_l \propto 1/\sqrt{l}$, and the "nominal" density anomalies in each layer scale with $1/\sqrt{l}$ compared with the "actual" density anomalies. Optionally, thermal boundary layers of thickness d_t and d_b, are added at the top and bottom. With these assumptions, the expected value of $\langle P_l \rangle$ is

$$E[\langle P_l \rangle] = \frac{1}{2}\left(\frac{3\widehat{\Delta\rho}}{(2l+1)\bar{\rho}}\right)^2 \left[\frac{N}{l}\sum_{i=1}^{N}(K(r_i)\rho_0(r_i)d)^2 + \left(C_t\sum_{i=1}^{N}K(r_i)\rho_0(r_i)d\left(1-\mathrm{erf}\left(\frac{r_E-r_i}{d_t}\right)\right)\right)^2 + \left(C_b\sum_{i=1}^{N}K(r_i)\rho_0(r_i)d\left(1-\mathrm{erf}\left(\frac{r_i-r_{CMB}}{d_b}\right)\right)\right)^2\right] \tag{4}$$

Here $d = (r_E - r_{CMB})/N$ is the layer thickness, and C_t and C_b are measures of the magnitude of density anomalies in the boundary layers relative to the bulk mantle.

2. Density structures inferred from mantle tomography models: We use a constant conversion factor between relative density and velocity variations $(\delta\rho/\rho)/(\delta v_s/v_s) = 0.3$ [*Karato*, 1993]. In most cases, we consider velocity variations only below depth 150 km. This conversion as a function of depth is rather uncertain, and with the wrong conversion, even a "correct" velocity and viscosity model would give the wrong geoid spectrum: *Hager and Richards* [1989] and *Panasyuk and Hager* [2000] discuss further how the choice of velocity-density conversion is closely related to the choice of seismic velocity model and viscosity model.

3. Density structure inferred from subduction history.

[7] We compare our model results with the power spectrum of JGM2G [*Nerem et al.*, 1994], in a version provided by S. Panasyuk (pers. comm.). Like *Hipkin* [2001], this version uses the hydrostatic equilibrium of the rotating Earth as reference shape, as is most appropriate in a geodynamic context. The "depth to source" analysis of *Hipkin* [2001] suggests significant contributions from density anomalies in the lithosphere at higher degrees. Therefore, we restrict our analysis to spherical harmonic degrees $l \leq 31$.

3. Results

[8] Results for $\langle P_l \rangle$ and $E[\langle P_l \rangle]$ are shown in Figure 2. They are "downward continued" to depth $d_{670} = 670$ km by multiplying them with $[r_E/(r_E - d_{670})]^{2l}$. This is merely a matter of presentation, as in this way, the range of values is approximately minimized. For the plots of $E[\langle P_l \rangle]$, $\widehat{\Delta\rho}$ is used as a free parameter, essentially allowing us to slide the curves up and down in the plot. In the top left panel, the lightly shaded region estimates the standard deviation of $E[\langle P_l \rangle]$ for the continuous line. Although these error bounds are very optimistic (we have ignored uncertainties in the kernels from, e.g., lateral variations in viscosity), 22 out of the 31 points (71%) from the observed gravity spectrum lie within the shaded region - which is expected statistically.

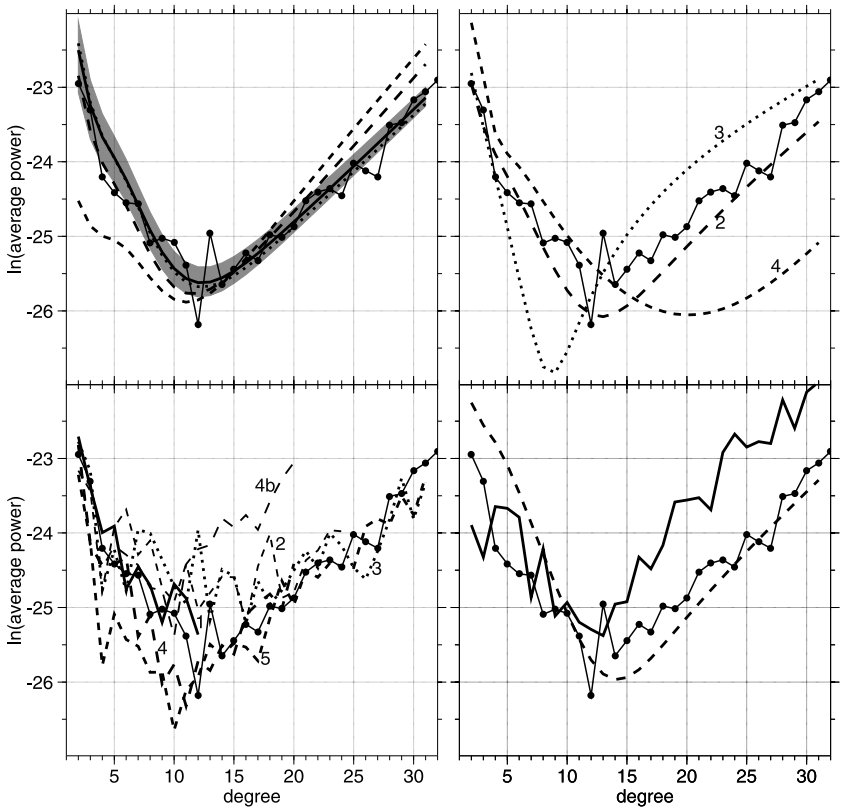

Figure 2. Observed and computed gravity power spectra. All values are multiplied by $[r_E/(r_E - d_{670})]^{2l}$. Observed values of $\langle P_l \rangle$ are shown in each panel as filled circles connected with a thin solid line. Note the breaks in slope at $l \approx 4$, 12. Computed values of $E[\langle P_l \rangle]$ or $\langle P_l \rangle$, are also plotted as solid lines. Top left: Results for viscosity structure (1) (see Figure 1) and different assumptions about random mantle density anomalies: Continuous line: $C_t = C_b = 0$. For this case, the region between $E[\langle P_1 \rangle](1 + 1/\sqrt{2l+1})$ and $E[\langle P_1 \rangle](1 - 1/\sqrt{2l+1})$ is drawn in light shading. Long-dashed line: $C_t = C_b = 3$, $d_t =$ 150 km, $d_b = 300$ km. Short-dashed line: Factor $1/\sqrt{l}$ is omitted in equation (3). Dotted line: Factor $1/\sqrt{(l+1)(2l+1)}$ in equation (3) is replaced by $1/(2l+1)$. For the latter two cases, again $C_t = C_b = 0$. Top right: Results for random mantle density anomalies, $C_b = C_t = 0$, and mantle viscosity structures (2)–(4) (see Figure 1). Numbers are indicated on curves. Bottom left: Results for different tomography models: 1 = S12WM13 [*Su et al.*, 1994], 2 = SAW24B16 [*Mégnin and Romanowicz*, 2000] 3 = SB4L18 [*Masters et al.*, 2000], 4 = S20RTS [*Ritsema and Van Heijst*, 2000], 5 = S. Grand's model, obtained in May 2002 from ftp://bratsche.geo.utexas.edu/outgoing/steveg), a development of *Grand et al.* [1997]. Model 4 is additionally shown with with conversion factor 0.3 through the entire mantle (labelled (4b)). Bottom right: Continuous line: Result for the slab density model of *Steinberger* [2000], obtained with viscosity structure (5). The dashed line gives the corresponding result for random mantle density anomalies and $C_b = C_t = 0$.

Therefore the thick solid line is an appropriate fit to the observed gravity spectrum. A qualitative explanation for this shape can be attempted based on the geoid kernels: They are a measure of how much a density anomaly at a given depth contributes to surface gravity. We tentatively relate the upper-mantle negative minima of the geoid kernels (right hand panel of Figure 1) for $l > 7$ to Hipkin's upper mantle white noise depth, the mid-mantle positive maxima of the kernels to the lower mantle white noise depth, and the lower-mantle negative minima for $l = 2$ and 3 to the poorly constrained lowermost mantle white noise depth. Obviously this relation is not straightforward; among other factors, the density anomaly spectrum assumed here is not a white but "pink" or "red" noise gravity source. Other curves in the top left panel of Figure 2 show effects of thermal boundary layers, and forms of $\sigma(l)$ different from that in equation (3): Whereas including a bottom boundary layer changes results very little, considering a top boundary layer tends to steepen the slope of $E[\langle P_l \rangle]$ for $l \gtrsim 15$. Simplifying equation (3) by replacing the factor $1/\sqrt{(l+1)(2l+1)}$ by $1/(2l+1)$ produces little change. However, if we omit the factor $1/\sqrt{l}$, i.e. assume that the average radial extent of an anomaly is independent of, rather than inversely proportional to its degree l, the fit significantly deteriorates.

[9] The top right panel of Figure 2 compares results for different viscosity structures. Although all of these were derived from optimizing the fit to the geoid, the predicted gravity spectra differ considerably, and only viscosity structure (2) yields a similar spectrum to (1). This indicates that the gravity spectrum may well be useful in addition to geoid or gravity itself as a constraint on mantle flow models. The bottom left panel shows results for various tomography models. Again, results differ considerably from each other. Comparison of cases (4) and (4b) shows again the strong dependence on the density anomaly strength in the top thermal boundary layer. The bottom right panel gives an example of how a geodynamic model tends to over-predict anomalies for $12 \lesssim l \leq 31$ compared with those for $2 \leq l \lesssim 12$.

4. Conclusions

[10] The results obtained leave us in a somewhat paradoxical situation: The "first guess" simplest model, based on a mantle viscosity structure that had been obtained in a previous, independent effort, and a very simple model of random density anomalies, gives an almost perfect fit to the observed gravity spectrum up to $l_{max} = 31$: Spectral range and slope of all straight-line segments of the observed gravity spectrum are well fit. Efforts to make the model more "realistic", such as including the effects of thermal boundary layers, worsen the fit. Gravity spectra predicted based on seismic tomography models differ considerably from each other. Neither they nor a geodynamic model based on subduction history fit the observed spectrum as well as our simplest "random source" model. Results based on full convection models were not considered: While the long-wavelength flow and density structures ($l \lesssim 12$) may be modelled realistically by imposing plate motions, computations at the presently accessible Rayleigh numbers are expected to over-predict intermediate-wavelength $12 \lesssim l \lesssim 31$ and under-predict short-wavelength structure. Thus a similar misfit as for the subduction model (Figure 2, bottom right) is expected (S. Zhong, pers. comm.). However, both the viscosity structure and the spectral dependence of density anomaly magnitude that we have used are based on models of seismic tomography. We interpret this finding such that mantle tomography models do tell us something about the internal density and flow structure of the Earth, especially on a very large scale, but that we are still far from quantitative knowledge of the Earth's mantle density anomalies, especially on a smaller scale: For example, with mantle viscosity structure (1) in combination with tomography model (3) the geoid can be fit quite well (variance reduction >70%). This good fit is however largely achieved by fitting the very low degrees ($l = 2$ and 3) very well. Figure 2 shows that for degrees 2 and 3 the actual spectrum and the modelled spectrum for tomography model (3) do in fact agree very well, but that for higher degrees the agreement gets increasingly worse. Of course, our "first guess" model is likely to be only one of many that can give an equally good fit to the observed gravity spectrum. A more systematic search through parameter space would be required to map out which models are compatible with the observed gravity spectrum as well as other constraints.

[11] A major omission from our study has been the neglect of the effects of lateral variations in mantle viscosity. To obtain a good fit to the spectrum, part of the modelled density spectrum must compensate for that part of the geoid that is in reality produced by mode coupling. This shortcoming of the present model needs to be kept in mind, and will be addressed further in future work. We anticipate that in the future the gravity spectrum can serve as an additional constraint to mantle flow and convection models, in much the same way as presently geoid, heat flow, core-mantle boundary topography etc., are used.

[12] **Acknowledgments.** We thank Shijie Zhong and John Wahr for discussion of ideas, Peter Molnar for comments on the manuscript, Arthur Calderwood for supplying his mineral physics models, Svetlana Panasyuk for supplying gravity coefficients in digital form, all the authors of the tomography models for making their models publicly available, and Brad Hager and Roger Hipkin for constructive reviews. Figures were prepared using GMT graphics [*Wessel and Smith*, 1995].

References

Becker, T. W., and L. Boschi, A comparison of tomographic and geodynamic mantle models, Geochem, *Geophys. Geosyst.*, *3*, 2001GC000168, 2002.

Dziewonski, A. M., and D. L. Anderson, Preliminary reference Earth model, *Phys. Earth Planet. Inter.*, *25*, 297–356, 1981.

Forte, A. M., A. M. Dziewonski, and R. L. Woodward, Aspherical Structure of the mantle, tectonic plate motions, nonhydrostatic geoid and topography of the core-mantle boundary, in *Dynamics of the Earth's Deep Interior and Earth Rotation*, Geophys. Monogr. Ser., 72, edited by J. L. Le Mouël, D. E. Smylie, and T. Herring, pp. 135–166, AGU, Washington, D. C., 1993.

Grand, S. P., R. D. Van der Hilst, and S. Widiyantoro, Global seismic tomography: A snapshot of convection in the Earth, *GSA Today*, *7*, 1–7, 1997.

Hager, B. H., and M. A. Richards, Long-wavelength variations in Earth's geoid: Physical models and dynamical implications, *Phil. Trans. R. Soc. Lond. A*, *328*, 309–327, 1989.

Hipkin, R. G., The statistics of pink noise on a sphere: applications to mantle density anomalies, *Geophys. J. Int.*, *144*, 259–270, 2001.

Karato, S., Importance of anelasticity in the interpretation of seismic tomography, *Geophys. Res. Lett.*, *20*, 1623–1626, 1993.

Kaula, W. M., Material properties for mantle convection consistent with observed surface fields, *J. Geophys. Res.*, *85*, 7031–7044, 1980.

Masters, G., G. Laske, H. Bolton, and A. Dziewonski, The relative behavior of shear velocity, bulk sound speed, and compressional velocity in the mantle: Implications for chemical and thermal structure, in *Seismology and Mineral Physics*, Geophys. Monogr. Ser., 117, edited by S. Karato, pp. 63–87, AGU, Washington, D. C., 2000.

Mégnin, C., and B. Romanowicz, The shear velocity structure of the mantle from the inversion of of body, surface and higher modes waveforms, *Geophys. J. Int.*, *143*, 709–728, 2000.

Nerem, R. S., F. J. Lerch, J. A. Marshall, E. C. Pavlis, B. H. Putney, B. D. Tapley, R. J. Eanes, J. C. Ries, B. E. Schutz, C. K. Shum, M. M. Watkins, J. C. Chan, S. M. Klosko, S. B. Luthcke, G. B. Patel, N. K. Pavlis, R. G. Williamson, R. H. Rapp, R. Biancale, and F. Nouel, Gravity model development for TOPEX/Poseidon: Joint gravity models 1 and 2, *J. Geophys. Res.*, *99*, 24,421–24,447, 1994.

Panasyuk, S. V., and B. H. Hager, Inversion for mantle viscosity profiles constrained by dynamic topography and the geoid, and their estimated errors, *Geophys. J. Int.*, *143*, 821–837, 2000.

Richards, M. A., and B. H. Hager, Geoid anomalies in a dynamic Earth, *J. Geophys. Res.*, *89*, 5987–6002, 1984.

Ritsema, J., and H. J. Van Heijst, Seismic imaging of structural heterogeneity in Earth's mantle: Evidence for large-scale mantle flow, *Science Progress*, *83*(3), 243–259, 2000.

Steinberger, B., Slabs in the lower mantle - results of dynamic modelling compared with tomographic images and the geoid, *Phys. Earth Planet. Inter.*, *118*, 241–257, 2000.

Steinberger, B. M., and A. R. Calderwood, Mineral physics constraints on viscous flow models of mantle flow, *J. Conf. Abs.*, *6*, 2001.

Steinberger, B., and R. J. O'Connell, Advection of plumes in mantle flow: Implications for hotspot motion, mantle viscosity and plume distribution, *Geophys. J. Int.*, *132*, 412–434, 1998.

Su, W.-J., R. L. Woodward, and A. M. Dziewonski, Degree 12 model of shear velocity heterogeneity in the mantle, *J. Geophys. Res.*, *99*, 6945–6980, 1994.

Thoraval, C., and M. A. Richards, The geoid constraint in global geodynamics: Viscosity structure, mantle heterogeneity models and boundary conditions, *Geophys. J. Int.*, *131*, 1–8, 1997.

Wessel, P., and W. H. F. Smith, New version of the Generic Mapping Tools released, *Eos Trans. AGU*, *76*, 3291995.

B. Steinberger, CIRES, University of Colorado, Campus Box 216, Boulder, CO 80309-0216, USA. (bernhars@cires.colorado.edu)

R. Holme, Department of Earth Sciences, University of Liverpool, 4 Brownlow Street, Liverpool, L69 3GP, UK. (holme@liv.ac.uk)